Lund University

Electro-optical Characterization of Semiconductor Nanowire Devices

Project work (30 ECTS)

Student: Neimantas Vainorius

Supervisor: Dan Hessman

Lund 2012

Abstract

Degradation of properties of semiconductor devices when layers of different materials are grown on top of each other is a common issue if their lattices are mismatched. Strain between them is reduced by creating defects like vacancies. This problem can be solved by growing structures, called nanowires, where stress is reduced radially. It is one of many reasons why it became a very interesting subject of investigation. We have used a Fourier transform spectrometer, a flexible instrument with high spectral resolution to investigate single InP nanowires with different doping, where no blue shift corresponding to state filling effect was observed, and the electro-optical properties of GaSb/InAsSb/InAs far infrared photodetectors. Also, electroluminescence of InP nanowire based light emitting diodes with a radial InP/InAsP/InP quantum well was studied. Broad spectrum, due to a non-uniform width of the quantum well, with two peaks at 1.46 eV and 1.57 eV was measured.

1. Table of contents

2. Introduction

A vast variety of electronic devices is used nowadays. Most of them are made of semiconductors and everybody now understands the importance of these materials. However, in the beginning development of semiconductor physics was quite slow and started in 1821, when T. J. Seebeck has discovered semiconductor properties of PbS. It took 90 years to introduce a term "semiconductor" and successful fabrication of the first transistor in 1947 led to the birth of a new era of semiconductor material based electronic and optoelectronic devices.

Huge amount of possibilities, especially in features related to semiconductor interaction with light, are offered the group III-V compound semiconductors. Many of them are known as direct band gap materials, so emission and absorption of photons are more favorable compared to indirect bang gap semiconductors where phonons are needed due to conservation of momentum. By changing proportions of the materials in binary, ternary or quaternary compounds properties like band gap or mobility can be easily tuned. This led to development of complex heterostructure solar cells, light emitting diodes emitting from infrared to ultraviolet light and other useful devices.

Growth of heterostructure is a complex process, where lattice matching materials are needed in order to avoid strain between separate layers. Due to this strain defects are introduced and properties of the fabricated device are degraded. One way to avoid this is to grow structures, called nanowires, where strain relaxation is reduced radially. This gives defect free semiconductor heterostructure and the possibility to grow them on top of silicon with intention of easy integration with already existing Silicon technology. Another advantage of nanowires is huge surface to volume ratio which is very attractive for light detection applications.

Due to the advantages and applications mentioned above various properties of semiconductor nanowires are widely studied. In this work a Fourier transform spectrometer was used for spectral photocurrent measurements. It is a fast and powerful tool allowing detailed investigation of material with high spectral resolution. Spectral photocurrent experiments allow exploring the band structure of semiconductors. For nanowire light emission experiments, a grating spectrometer was used in order to investigate the spectrum of the emitted light.

The main purpose of this project work was to investigate the electro-optical properties of already fabricated differently doped InP nanowire FETs, GaSb/InAsSb/InAs far infrared photodetectors and InP nanowire based light emitting diodes with InP/InAsP/InP radial quantum well.

3. Theory

3.1. *p-n* junction

One of the most important "building blocks" of semiconductor devices is the *p-n* junction or diode. It is irreplaceable for devices, such as solar cells, light emitting diodes, detectors, integrated circuits, etc. A *p-n* junction is formed at the interface of *p* and *n* doped semiconductor crystal or between two different materials.

In an abrupt *p-n* junction without bias applied, an equilibrium condition is reached. Holes from the *p*-doped crystal side diffuse over the *p-n* junction to the *n*-doped side where they recombine with electrons. As holes diffuse, they leave negative acceptor ions in the *p* region. The same process occurs with electrons. They diffuse from *n* to *p* region leaving positively charged donors. Due to these two processes, the region around the *p-n* junction is depleted of majority carriers. This region is called depletion region.

Ionized dopants create space charge region and potential difference between *p* and *n* doped material, which is known as the diffusion voltage [1], V_D:

$$V_D = \frac{kT}{e} ln \frac{N_A N_D}{n_i^2}, \quad (1)$$

where n_i is the intrinsic carrier concentration, N_D and N_A is the donor and acceptor concentration of the semiconductor, respectively. Electric field generated by space charge tends to cancel out carriers diffusion. So, there is a clash of two contrary processes and both of them counteract with each other.

When a reverse bias (positive voltage to the *n*-type and negative voltage to the *p*-type material) is applied, the majority of the carriers move away from the *p-n* junction due to electric force. The width of the depletion region increases so the junction barrier increases as well [2].

Typical devices working under reverse bias condition are light detectors. If the photon is absorbed in the depletion region, the generated carrier pair is then separated by the electric field. To make the device more sensitive, an intrinsic semiconductor between the highly *n*-doped and *p*-doped regions or heterostructure is used.

Under forward bias condition electrons drift to *p*-type and holes drift to n-type region more easily because the junction barrier is lowered. This effect is used in light emitting diodes (LED) where carrier injection to active region is needed.

3.2. Burstein-Moss shift

In the case of an intrinsic semiconductor no states in a conduction band are filled with electrons at low temperature and the Fermi level is between the valence and conduction bands. If an electron is excited to the conduction band, it will jump from the bottom of it to the valence band emitting a photon of exactly the same energy as the semiconductor band gap.

In an *n*-doped semiconductor, the Fermi level of the electrons moves up closer to conduction band and when doping is high enough, the Fermi level is found in the conduction band. Below about 4*kT* of the Fermi level, all states are filled with electrons (Fig. 1 shown in grey). So, the distribution function is changed drastically [3]. Due to this, higher photon energy is needed to excite an electron ($\hat{k}$ indicates the lowest possible optical transition due to absorption or emission). This phenomenon is known as Burstein-Moss shift.

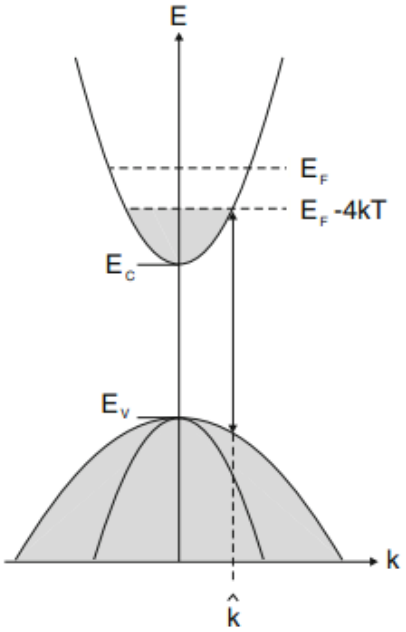

Fig. 1. Schematic ilustration of Burstein-Moss Shift [3].

Besides energy shift in the conduction band due to the state filling effect, corresponding shift is visible in valence band.

Doping is not the only factor that can cause Burstein-Moss shift. Another possible reason might be strong optical excitation. In this case electrons are excited to the conduction band by absorbing photons. If light intensity is high enough then carrier excitation rate is higher than recombination. This means that empty states is filling up with electrons, which is known as a state filling effect.

3.3. Introduction to Fourier transformation spectroscopy

Electromagnetic radiation and material interactions are well known now. Radiation can be absorbed or scattered by atoms or molecules, reflected by material surfaces, excited atoms can emit light and then return to the lowest energy state. All these processes give big amount of possibilities to investigate materials from different perspectives.

3.3.1. Fourier transformation

The band gap of semiconductors varies form 0.18eV (InSb) to 3.6eV (ZnS) or even 5.5eV (diamond). This corresponds to 6900, 344 and 225 nm wavelength, respectively [4]. So, for a semiconductor optical investigation infrared (IR) and visible light are the most suitable. A very interesting property of material is absorption of light of a specific wavelength which is used for semiconductor band structure studies.

For spectral measurements of absorption a Fourier transform spectrometers are often used due to their high resolution, short measurement times and wide spectral range. The main part of these instruments is an interferometer. The Michelson interferometer's scheme is shown in a picture below (Fig. 2). Light emitted by the light source goes to the beam splitter. The beam splitter divides light into two beams of the same amplitude. One of the splitted beams goes to a stationary mirror and another to a moving mirror where they are reflected back to the beam splitter. After the beam splitter the intensity of beams are reduced by 50% again and they interfere with each other. Interfered radiation goes to the detector where an interferogram (signal intensity dependence on optical path difference (OPD)) is recorded. In order to extract a spectrum (amplitude dependence on frequency) from the interferogram Fourier transformation is used.

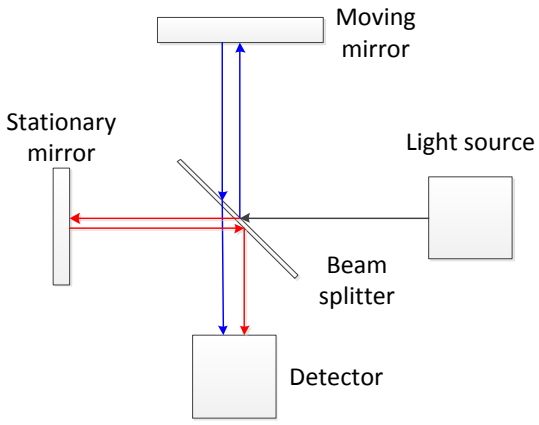

Fig. 2. Schematics of Michelson interferometer

With the movement of one mirror one beam must travel a longer distance than the other. Due to uniform speed of light, we can say that one beam travel longer in time by τ. If we consider monochromatic light:

$$\psi_1(\vec{r},t) = a \cdot e^{i(\omega t+\vec{k}\vec{r})}, \tag{2}$$

$$\psi_2(\vec{r},t) = a \cdot e^{i(\omega(t+\tau)+\vec{k}\vec{r})}, \tag{3}$$

where a is amplitude, ω – frequency, $\vec{k}$ – wave number, $\vec{r}$ – traveling direction of the wave. After recombination of these two waves at the beam splitter, the result is:

$$\psi_{total}(\vec{r},t) = \psi_1+\psi_2 = a \cdot \left(1 + e^{i\omega\tau}\right) \cdot e^{i(\omega t+\vec{k}\vec{r})} \tag{4}$$

The part of the last equation that is of interest to us is amplitude of the wave, because detectors record only intensity of light. We can write that $\sigma = \frac{\omega}{2\pi c}$ and $x = c\tau$ that, σ and x are wavenumber and optical path difference between the two mirrors of the interferometer, and then $\omega\tau = 2\pi\sigma x$. The amplitude is thus given by:

$$A = a \cdot \left(1 + e^{i2\pi\sigma x}\right). \tag{5}$$

Intensity *I* can be defined as *AA**. Also we are only interested in the AC component of the beam. After few assumptions we made, the intensity of monochromatic light can be described as

$$I = 2a^2\cos(2\pi\sigma x). \tag{6}$$

follows:

If we consider polychromatic light, then we have to integrate (5) over all wavenumbers, taking into account that amplitude of a light at different wavelengths might be different:

$$I(x) = \int_{-\infty}^{\infty} S(\sigma)\, e^{-i2\pi\sigma x} d\sigma, \tag{7}$$

where $S(\sigma) = a^2(\sigma)$ and is called spectral intensity or spectrum. Also, it is correct to write:

$$S(\sigma) = \int_{-\infty}^{\infty} I(x)\, e^{i2\pi\sigma x} dx, \tag{8}$$

The last two equations are mathematical expressions of spectrum $S(\sigma)$ and interferogram $I(x)$ related by Fourier transformation. More brief mathematical derivation and Fourier transform description is introduced by P. Davis [5], P. Griffits [6] and D. Wunch in her doctoral thesis [7].

3.3.2. Phase errors and corrections

The true spectrum is real and positive. This means that the interferogram must be symmetric and the Fourier transform of sine (6 and 7 equations) should be zero. In order to get perfect interferogram and spectrum OPD must be varied from zero to infinity. That is obviously impossible. Due to this, the spectrum might be deformed (line shape, position, size and signal-to-noise ratio). This is one of many possible reasons related to experimental (one-sided interferogram measurement instead of double-sided), instrumental (light source signal intensity is not truly stable) and computational limitations that introduces asymmetries to the interferogram. So, in a real spectrum, some information is shifted to the imaginary part. To reconstruct spectrum from asymmetric interferogram, complex Fourier transformation must be used [5].

The most common phase error is related to the different response of optical components to different wavenumbers and due to the fact, that the zero path difference (ZPD) position is not sampled. This adds an extra term $\epsilon(x)$ to equation (6) (the following mathematical treatment is borrowed from [7]):

$$M(x) = \int_{-\infty}^{\infty} S(\sigma)\, e^{-i\left(2\pi\sigma x + \epsilon(x)\right)} d\sigma. \tag{9}$$

There are methods proposed for this error correction, Forman's method being one of them [8]. Using this method an asymmetric single-sided interferogram measured with FTS can be symmetrized.

The first aim is to compute the phase spectrum $e^{-i(\epsilon(x))}$. In order to do that a double sided interferogram is needed, because the phase spectrum describes how asymmetric an interferogram is. It is calculated by taking the Fourier transform of double sided interferogram made of equal number of points taken from both sides of a single sided interferogram $M(x)$. After taking the Fourier transform we get low-resolution complex spectrum $m_s(\sigma)$:

$$m_s(\sigma) = \int M_s \, e^{2\pi i \sigma x} dx. \tag{10}$$

$\epsilon(x)$ could be calculated using Euler's identity $\left(e^{ix} = cos(x) - isin(x)\right)$:

$$m_s(\sigma) = S_s(\sigma)e^{-i\epsilon(\sigma)} = S_s(\sigma)\{\cos(\epsilon(\sigma)) - i\sin(\epsilon(\sigma))\}, \tag{11}$$

where $S_s(\sigma)$ is low-resolution real spectrum. By dividing imaginary part ($\Im[m_s(\sigma)]$) by real part ($\Re[m_s(\sigma)]$) we get:

$$-\tan(\epsilon(\sigma)) = \frac{\Im[m_s(\sigma)]}{\Re[m_s(\sigma)]}, \tag{12}$$

and:

$$\epsilon(\sigma) = \arctan\left(\frac{\Im[m_s(\sigma)]}{\Re[m_s(\sigma)]}\right). \tag{13}$$

Next step is to define a phase interferogram $F(x)$:

$$F(x) = \int_{-\infty}^{\infty} e^{i\epsilon(\sigma)} \, e^{-2\pi i \sigma x} d\sigma. \tag{14}$$

In order to suppress spurious oscillations that arrive from the Fourier transformation of the boxcar function (we have multiplied primal one-sided interferogram with this function to get low resolution double-sided interferogram), Forman suggested using apodizing function [8]:

$$\left[1 - \left(\frac{\tau}{n}\right)^2\right]^2, \tag{15}$$

where τ is a vector, *n* – number of points taken around ZPD.

After phase spectrum was apodized, we convolute it with one-sided interferogram $M(x)$ to get phase corrected interferogram:

$$I(x) = M(x) * F(x). \tag{16}$$

All in all, according to the mathematical expressions above the asymmetric interferogram can be corrected by convolving it with the inverse Fourier transform of the phase spectrum $e^{i\epsilon(\sigma)}$.

4. Preparations for measurements and experimental setups

4.1. Preparations for measurements

Before doing experiments some preparations had to be done. First of all, software for IV and time/temperature dependence measurements was written using the graphic programing software package LabView 9. Also, Bomem Fourier transform spectrometer, which electronics was replaced, controlling software was upgraded for more flexible experiments including phase correction of the measured interferogram (see Fig. 3). For a phase correction the Forman's algorithm, which was described above, was used (chapter 3.3.2). Similar algorithms were used in renewed FTS by D. Wunch [7], [9].

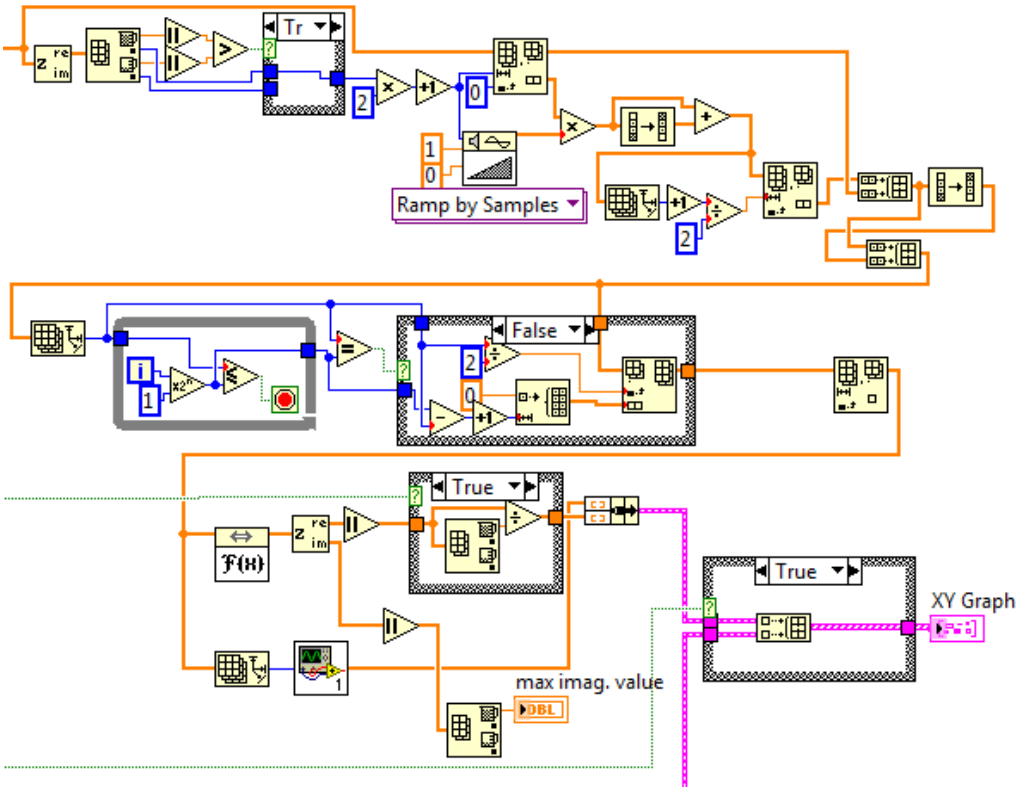

Fig. 3. Fragment of a program responsable for phase correction.

In order to do experiments with FTS at low temperatures, specific sample holder and temperature related, including pumps for vacuum, equipment was needed. First step before doing measurements was to prepare experimental setup. All different setups will be described below. For low temperature and temperature dependence measurements a helium cryostat was prepared. Different sets of windows were used for different samples and source characterization. For an InP

single nanowire measurements quartz and CaF_2 windows and for GaSb/InAsSb/InAs infrared detectors ZnSe outer with ZnS inner as well as CaF_2 (both windows) window sets were used.

4.2. Light source characterization

In order to perform an experiment of the spectral photocurrent correctly, the spectral distribution of light sources used must be known. Light source characterization was accomplished (Fig. 4). For this experiment deuterated triglycine sulfate or DTGS detector was used. The main aim of using this detector is its flat response characteristics in a broad range of the wavelengths.

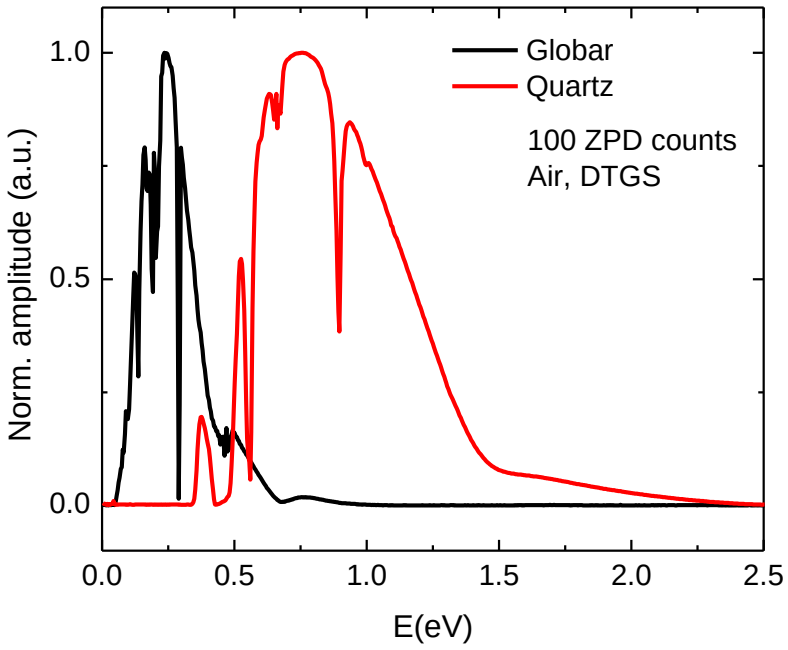

Fig. 4. Spectum of light sources.

Sharp dips visible in the spectra correspond to electromagnetic radiation absorption by air molecules (water, CO_2, etc.). To avoid wrong interpretation of measured spectrum experimentalist should be aware of absorption in the air or all the spectrometer system should be evacuated. The DTGS detector we used is not very sensitive above 1.2 eV, so the quarts spectrum of higher energies might be distorted.

4.3. Experimental setups

4.3.1. Photocurrent dependence on temperature experimental setup

Experiments were done where photocurrent dependence on excitation power was investigated. A Laser and filters were used for exciting InP nanowire and two distinct regions (linear and saturation) were shown [10]. In order to repeat the experiment and measure temperature dependence of the photocurrent in the two distinct regimes several different setups were prepared. One of them is shown in a picture below (Fig. 5). In the path of the strong laser a light chopper and some adjusting optics were placed. The sample was cooled by a liquid helium circulating inside the cryostat. In order to measure photocurrent, programmable DC source, low-noise preamplifier and lock-in amplifier was used. Data was recorded by a computer.

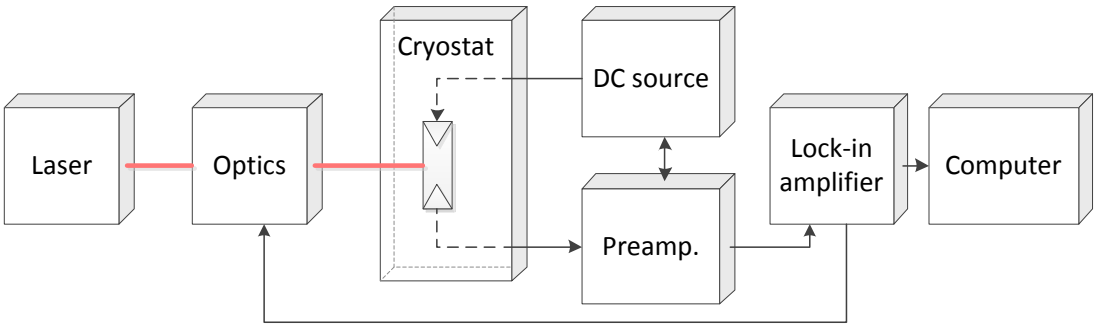

Fig. 5. Block diagram of experimental setup for temperature dependent measurements

For carrier optical excitation three different lasers were used in different setups. We have started with semiconductor diode laser which, as we find out, was not working properly and gave us 3 laser spots instead of one and strange interference pattern. Next we used an Ar^+ ion laser which however was not powerful enough to reach the saturation region. This region was reached with a supercontinuum light source[1]. However, this laser was not a perfect option for us due to the broad spectrum.

[1] Large spectral broadening of the laser is acheaved within the highly nonlinear fiber using powerful and short (4 ps) pulses.

4.3.2. Spectral photocurrent measurement setup

For spectral photocurrent measurements a Fourier transform spectrometer (FTS) was used. There was a possibility to select one of three light sources: a quartz lamp for visible and near infrared light, Hg lamp for UV and globar for mid and far infrared light. Light emitted by selected source goes through a Michelson interferometer as it was described before (3.3.1). After that it is focused on a biased sample inside cryostat that acts as a light detector. The generated photocurrent is converted to voltage by a low-noise current preamplifier (Stanford research systems model SR570). Then the amplified signal is sent to an analog-to-digital converter (ADC). A digital interferogram is read and transformed using the Fourier transformation algorithm by a computer (Fig. 6).

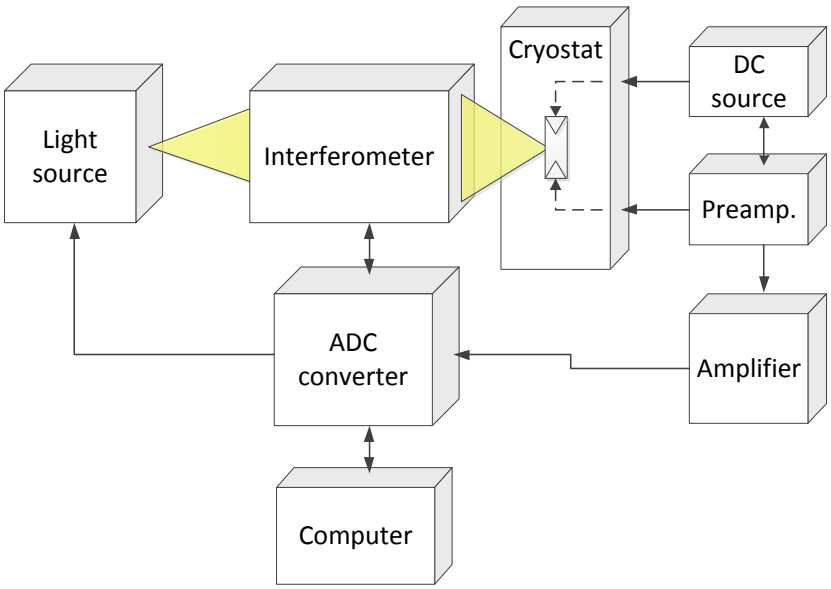

Fig. 6. Block diagram of spectral photocurrent measurement setup.

4.3.3. Electroluminescence experiment setup

A block diagram of the experimental setup for electroluminescence spectral measurements is shown in Fig. 7. A DC source was needed to apply forward bias on the sample. When the sample is forward biased, it emits light due to electrical carrier injection to an active region with quantum well

(the sample will be described more briefly in next chapter). In order to register and measure light wavelength a grating monochromator and CCD camera was used.

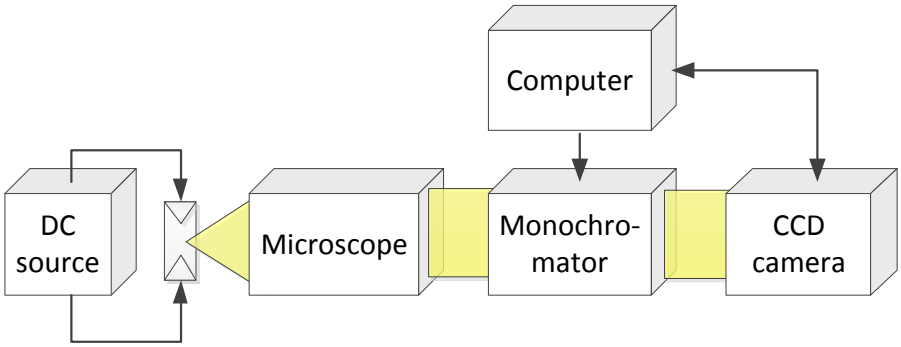

Fig. 7. Block diagram of electroluminescence measurement setup.

4.4. Sample description

4.4.1. Differently doped InP nanowires

Indium phosphide is a binary III-V semiconductor compound. In bulk it has a face-centered cubic crystal structure known as zincblende (ZB). The band gap is 1.42 eV at absolute zero temperature and it is changing with temperature as follows [11]:

$$E_G(T) = E_G(T=0) - \frac{\alpha T^2}{T+\beta}\,, \tag{17}$$

where $\alpha = 4.9 \cdot 10^{-4}$ eV/K and $\beta = 327$K.

However, usually in nanowire structure InP has a mix of ZB and wurtzite (WZ) [12]. Percentage of each type of crystal structure can be regulated by doping. For example, undoped nanowires contain similar proportions of both structures, but with increasing doping of S dopant WZ structure becomes dominant. WZ InP is not fully investigated, but some interesting properties are already known, for example, the existence of a second conduction band 0.24eV above the first one [13]. A mixture of ZB and WZ InP forms type 2 alignment. A picture below (Fig. 8) indicates spatial separation between electrons and holes. ZB structure acts as a trap for electrons and the conductivity is determined by the longest ZB segment [14].

Differently doped InP nanowires were grown by Metal Organic Vapor Phase Epitaxy (MOVPE). Then, scraped from the substrate using cleanroom paper, it was placed on a Si wafer with SiO_2 on top. Nanowires were contacted with Ti/Pd/Au to the highly hydrogen sulfide (H_2S) doped

regions to obtain ohmic contact (Fig. 9). In a table below doping of the investigated samples is shown:

Table 1. Dopent concentration of InP single nanowire samples.

	Anw	JWP26B	JWP31B	INPS
$n(\mathrm{cm}^{-3})$	$\approx 8 \cdot 10^{13}$	$\approx 5 \cdot 10^{18}$	$\approx 9 \cdot 10^{18}$	$\approx 10^{20}$

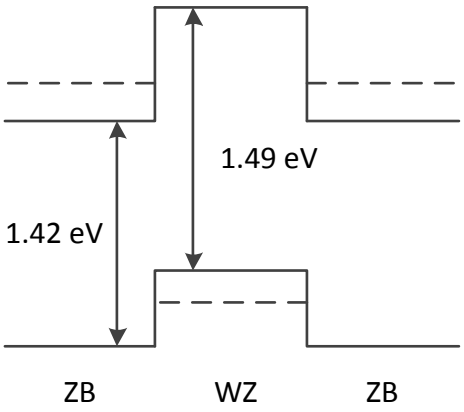

Fig. 8. Type 2 alignment of ZB and WZ InP.

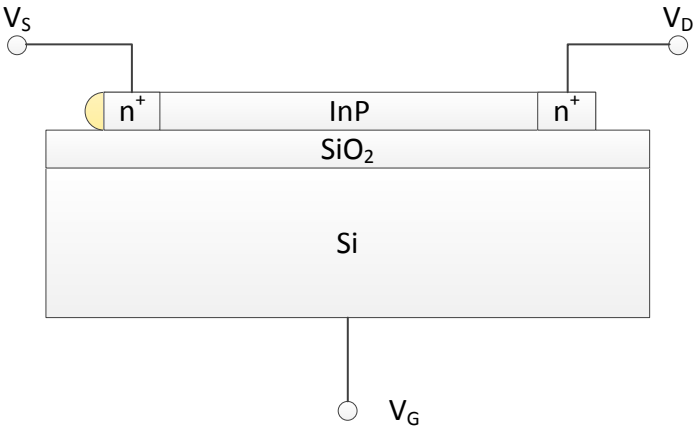

Fig. 9. InP nanowire sample schematic drawing.

An InP nanowire on Si wafer separated from it with SiO_2, acts as a conductance channel of a field effect transistor (FET). This means that current flowing through the nanowire can be easily changed with the gate voltage. Especially high sensitivity to gate voltage was observed in the intrinsic InP.

4.4.2. GaSb/InAsSb/InAs nanowires

InAsSb is a low band gap semiconductor. A Band gap varies from 107.6 meV ($InAs_{0.34}Sb_{0.66}$) to 354 meV (InAs) at room temperature. This material is promising candidate for far infrared detection applications. Due to large lattice mismatch and strain between the InAsSb and cheap substrate material defects are created during layer growth. One way to solve this issue is to grow nanowires where strain is relaxed through radial expansion. To investigate a possibility to use nanowires for long wavelength infrared detection GaSb/$InAs_{0.9}Sb_{0.1}$/InAs nanowire heterostructure were grown by MOVPE. Two different types of samples (single and multiple nanowires) were fabricated.

A single nanowire sample was prepared similarly to InP samples. This process was described in a previous chapter. A schematic image of it is shown in a picture below (Fig. 10). In this case *p-i-n* diode is formed using heterostructure of different materials (Fig. 11). If electrons and holes are genrated in an intrinsic InAsSb region, they are separated by internal electric field. This gives a change in current that is proportional to the light intensity.

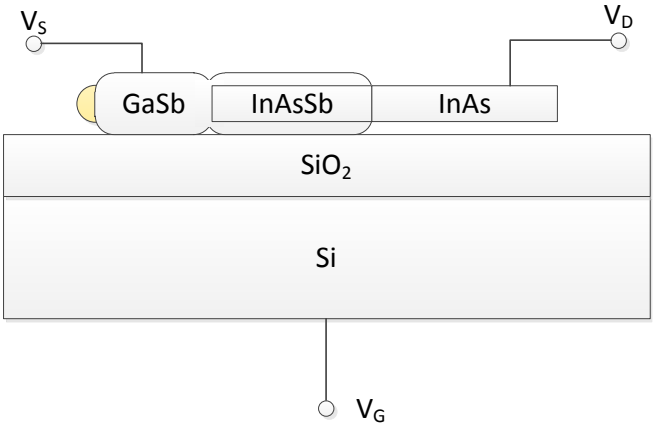

Fig. 10. Schematic drawing of single GaSb/InAsSb/InAs nanowire.

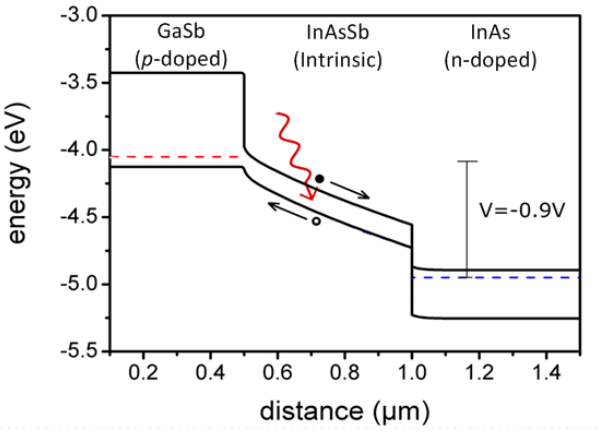

Fig. 11. Band diagram of the device 11.

One of advantages to use the heterostructure in this kind of devices is to have intrinsic or lightly doped material between two other semiconductor materials with larger band gap. Then dark current is reduced due to prevention of carriers to be excited in the heavily doped parts [15].

Real images of nanowires after growth and the single nanowire sample (s1c11g10) after fabrication taken by scanning electron microscope are shown in Fig. 12 and Fig. 13, respectively. A GaSb segment is visible on the top of the nanowires after growth due to a neck-like nick. However, after the sample fabrication this segment usually brakes off and nanowire is contacted to the thin GaSb shell (Fig. 13 top contact).

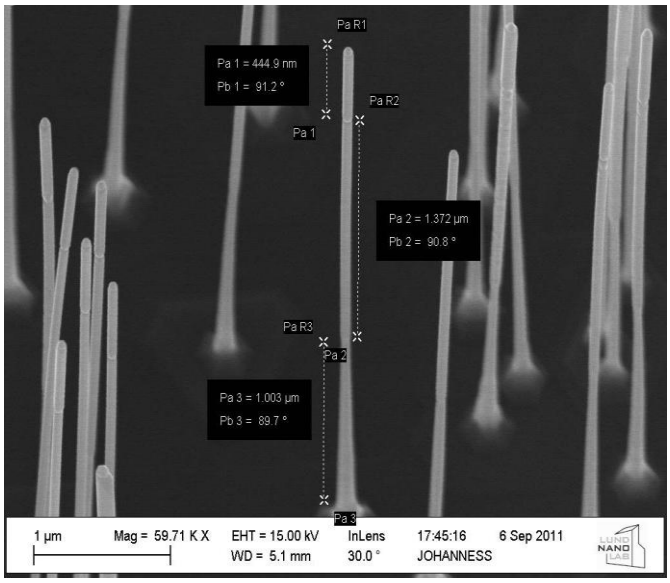

Fig. 12. SEM image of standing nanowires after growth.

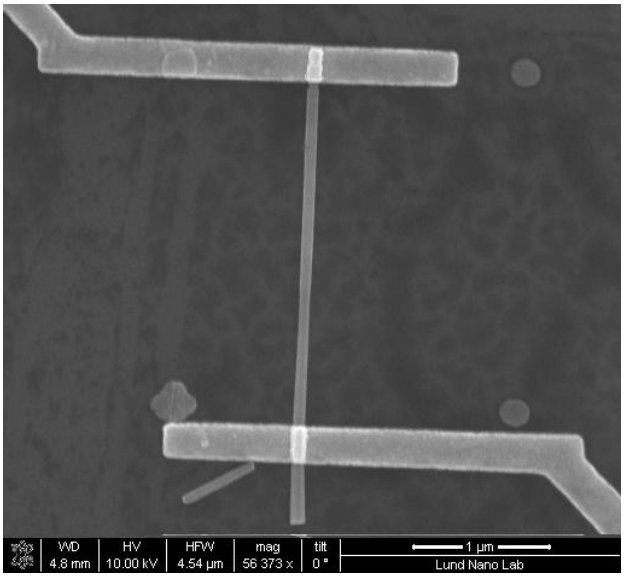

Fig. 13. SEM image of sample s1c11g10.

Samples with multiple nanowires standing in perpendicular to substrate were fabricated to have more nanowires connected in parallel (Fig. 14). On a thick high resistance Si substrate low resistance layer (300nm) of *n*-doped InAs was grown. This layer must be of good thickness, because it must be transparent to light and have good electrical properties at the same time. A nanowire structure in this case is similar to the single nanowires as discussed above.

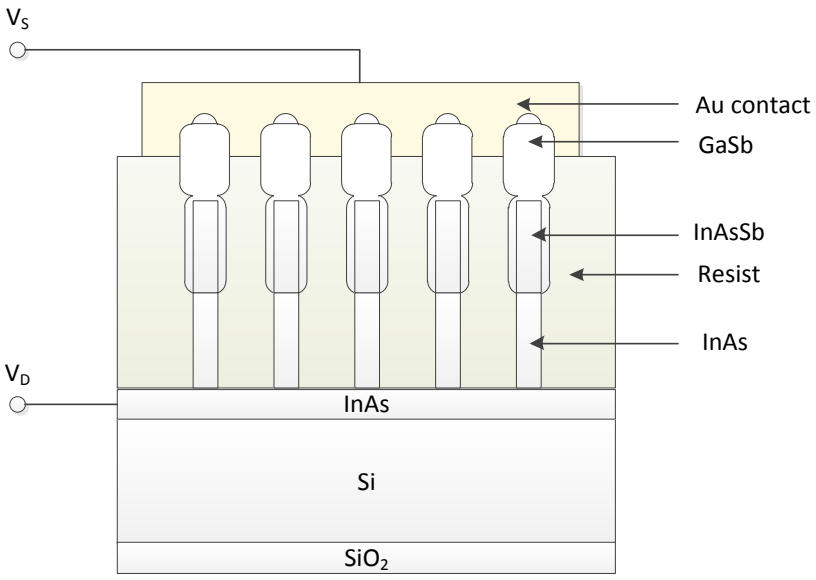

Fig. 14. Schematic drawing of GaSb/InAsSb/InAs multiple nanowires sampe.

After the growth nanowires, a next sample fabrication step was needed in order to contact them from the top (to the GaSb segment). First of all, all wires were buried under the resist (some of them fully, some not due to the non-uniform length) (Fig. 15). Then the resist was etched down to have a GaSb segment sticking out (Fig. 16). Both, the resist and nanowires were removed from the part of the sample before the top contact metallization. This step is needed in order to contact the InAs layer. A next stage of the sample fabrication is top 540nm thickness Ti/Au contact

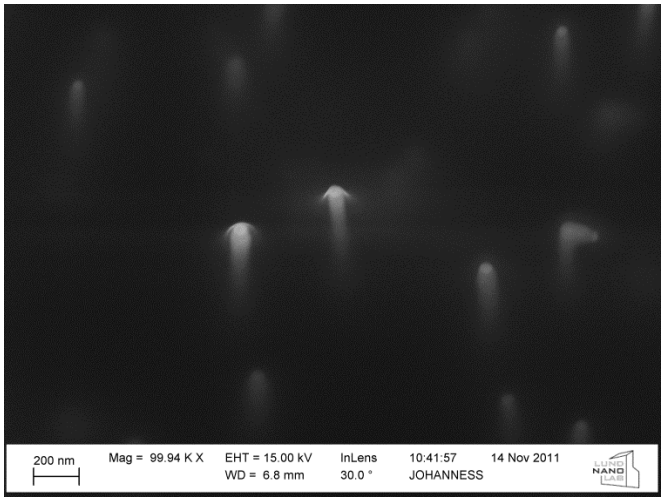

Fig. 15. Nanowires buried in the resist before etching (V7 sample).

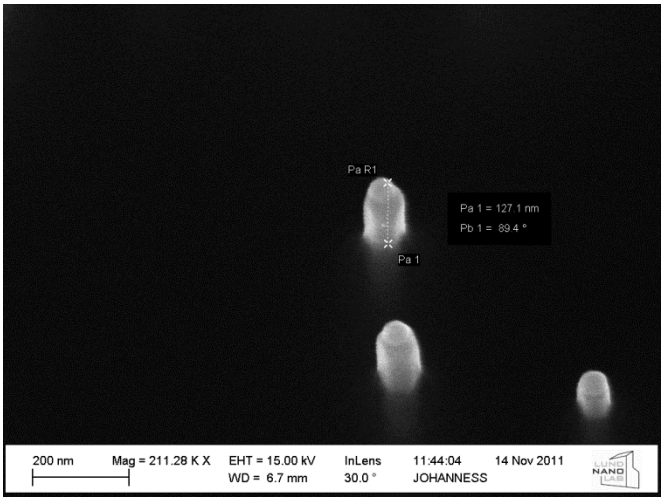

Fig. 16. Nanowires burried in the resist after eching (V7 sample).

evaporation using specific mask. Ti/Au was used to have good ohmic contact to *p*-type GaSb. The mask used gave a possibility to have different size top contacts allowing connecting different number of nanowires in parallel.

This sample was designed for illumination from the back side, because light cannot get through a thick gold top contact. A ceramic sample holder with a hole in the middle was used for this purpose.

4.4.3. InP nanowire based LEDs

InP is a direct band gap semiconductor material. It is promising for development of infrared optoelectronic devices such as light emitting diodes.

A simplified schematic drawing of the InP nanowire LED devices is shown in Fig. 17(a). For the device fabrication several important steps are needed. First of all, WZ InP nanowires with radial quantum well of 2 nm thickness were grown on the *n*-doped InP substrate. A core of the nanowire is *n*-type WZ InP semiconductor. An *i*-InP/*i*-$InAs_{0.2}P_{0.8}$/*i*-InP quantum well is formed and the *p*-InP

shell is used for a surface passivation and to contact the device for electrical and electro-optical studies (see Fig. 17 b). Next step is to deposit insulating SiO_2 layer on top of the wafer with nanowires and covering everything under the resist. Then the resist was etched a little bit below the

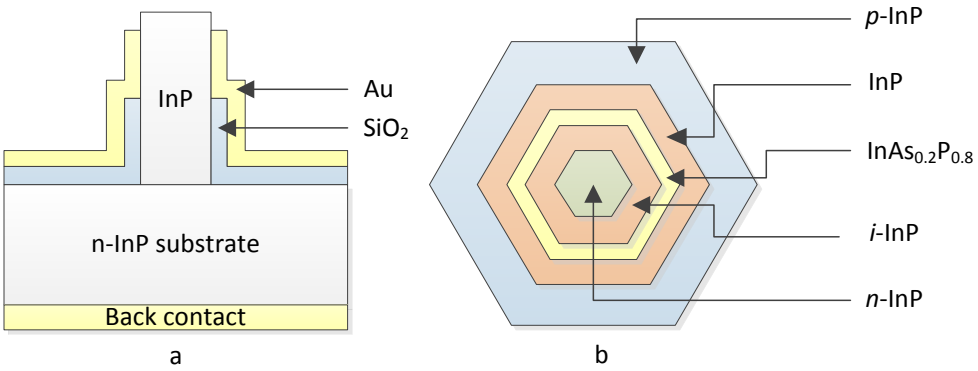

Fig. 17. Schematic drawing of InP nanowire based light emitting diode.

tip of the nanowires. After that the SiO_2 was removed to provide a space for metallization. After etching down all resist, gold was evaporated on the top of wires. Then few more steps were needed to remove gold from the top of the nanowires which should allow light to escape nanowire more easily.

5. Experimental results and discussion

5.1. InP nanowires with different doping

Several different experiments were performed on InP nanowires with different doping. The samples of the most interest were undoped InP single nanowires.

A photocurrent dependence on exciting light power was performed to repeat experiment described in [10]. For this measurement a powerful supercontinuum laser was used. Two different regions (linear and saturated) were visible and are shown in a picture below:

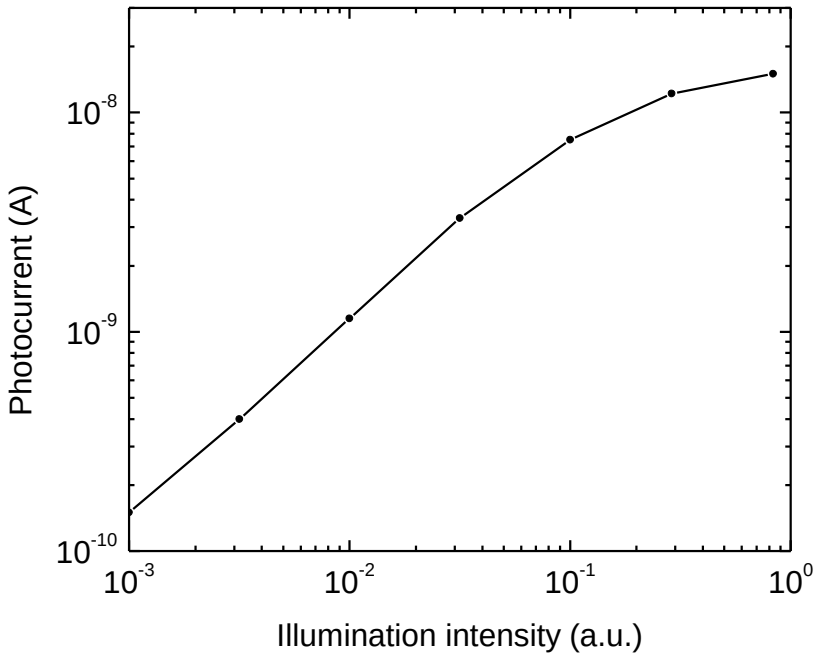

Fig. 18. PC as a function of incident light intensity of undoped sample (ANW18).

After convincing results of linear and saturation regions, setup for temperature dependence was prepared (see Fig. 5). Unfortunately, due to some problems no good data was measured. The main issue of this experiment was a thermal expansion of the sample holder stick with increasing temperature. We have approximately evaluated length difference taking into account stick length and material, between room temperature (RT) and low temperature (LT) ($\Delta L = \alpha \cdot L \cdot \Delta T$). The result we have got was around two millimeters. This means that with increasing temperature nanowire of our interest moves out of the laser spot. This fact is illustrated with our measurement data shown in Fig. 19. At LT we have optimized a laser spot position to get

the strongest signal. With increasing temperature stick gets longer and moves biased nanowire out of the spot resulting light intensity drop as well as the signal measured with a Lock-in amplifier.

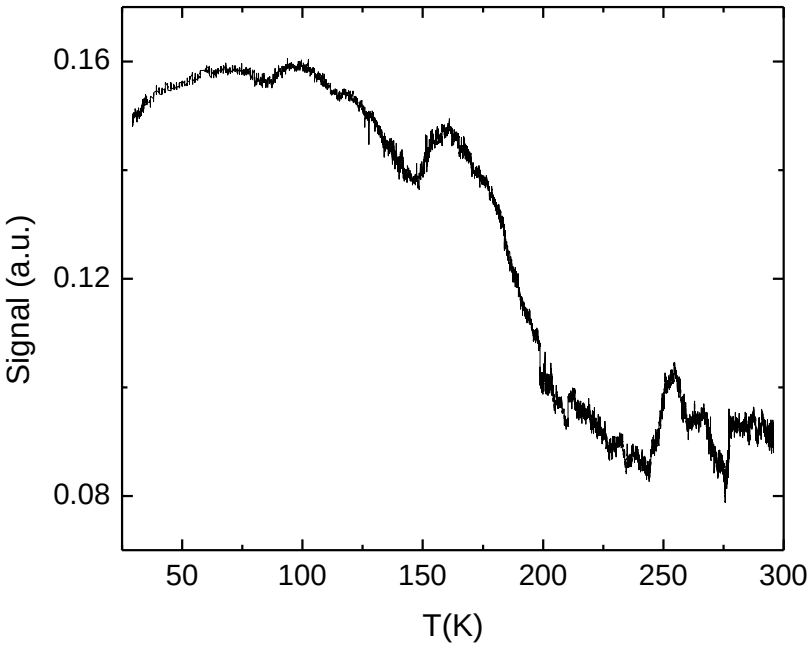

Fig. 19. Signal dependence on temperature.

After this measurement laser position was optimized again and the signal value increased close to the value at LT. One way to solve this problem was to defocus laser spot to make it bigger. But with defocusing laser, light intensity per area is getting lower. Here we encountered another problem – we could not reach saturation region anymore.

Another solution for the main issue of this experiment was to adjust laser spot during the temperature sweep. For this purpose we used a translation stage. This allowed us to change focus of a laser through lens and adjust spot in *x* and *y* directions. However, the SC laser was not good light source for this experiment, because less than half of the emission spectrum was used for carrier excitation and another part for sample heating which was not desirable effect. On the other hand, at that time we did not have another powerful enough laser (saturation region was reached only using this laser).

Due to too big errors this experiment did not gave us any favorable results. Furthermore, after few sweeps electrical properties of the sample changed. One of the reasons for that might be too high temperature of the sample due to the SC laser heating issue. If the temperature was high enough some of the molecules (water, etc.) could be evaporated from the surface of the sample.

All things considered, even when the nanowire moves out of the center of the beam, current does not change a lot neither in saturation region nor in linear. This indicates small current dependence on temperature which corresponds to a minor influence to conductivity of the phonon scattering. On the other hand, due to SC laser heating, temperature of measured nanowire is not well known and this could lead to misinterpreting results.

Another part of measurements related with these samples were spectral photocurrent measurements. In a picture below (Fig. 20) extracted conductivity of all investigated samples is shown. As it was expected, a conductivity of the nanowire increases with doping. Due to high current of the heavily doped samples (JWP31B and inps) no spectral photocurrent was measured.

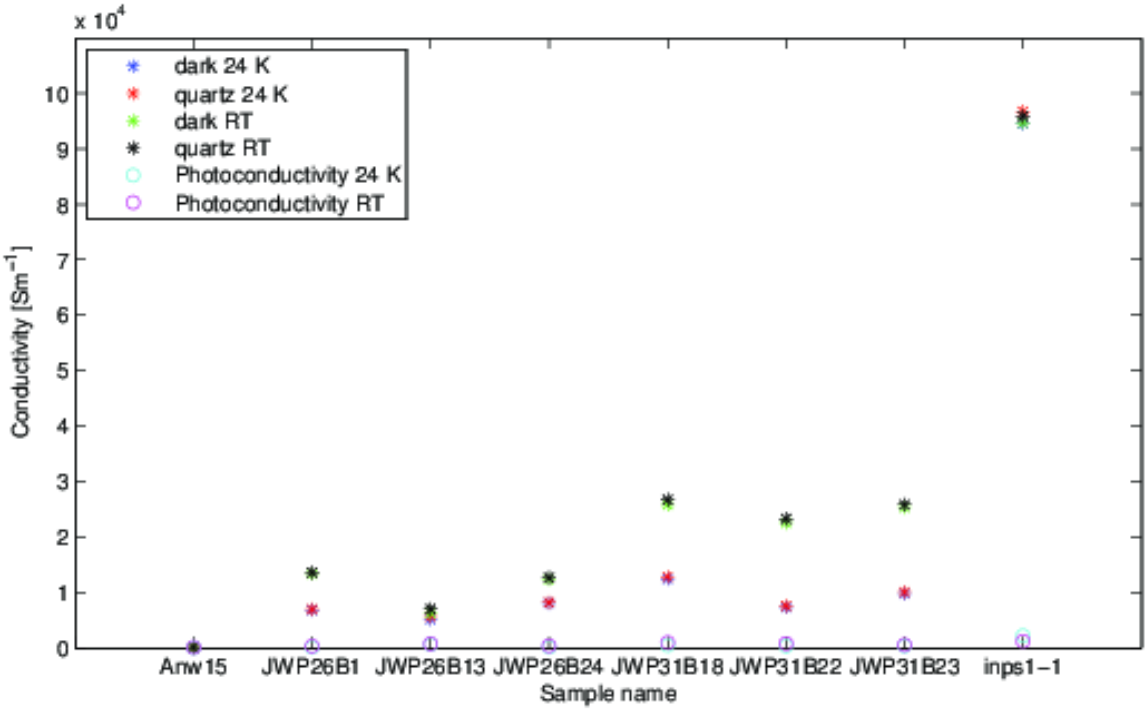

Fig. 20. Conductivity under different conditions of investigated samples.

The conductivity as a function of temperature for differently doped samples is shown in Fig. 21. Nanowires of lower doping act as a semiconductor - conductivity increases with increasing temperature due to the thermal excitation of carriers. But the heavily doped sample (S dopant is saturated) behave like a metal at higher temperatures (green curve). Here conductivity increases when temperature decreases, because of reduced phonon scattering. Conductivity of metals should saturate due to 'frozen' phonons at low temperatures. In our case it starts to decrease from 86K. One possible explanation of this phenomenon might be related to excitons. An exciton binding energy to the ionized shallow donor is 6.7meV (7.47meV) [16], which is close to the thermal energy

of 86 K mentioned before, meaning that at lower temperatures electrons are bound to donors. Due to this, number of free carriers as well as conductivity is decreased of the nanowire sample.

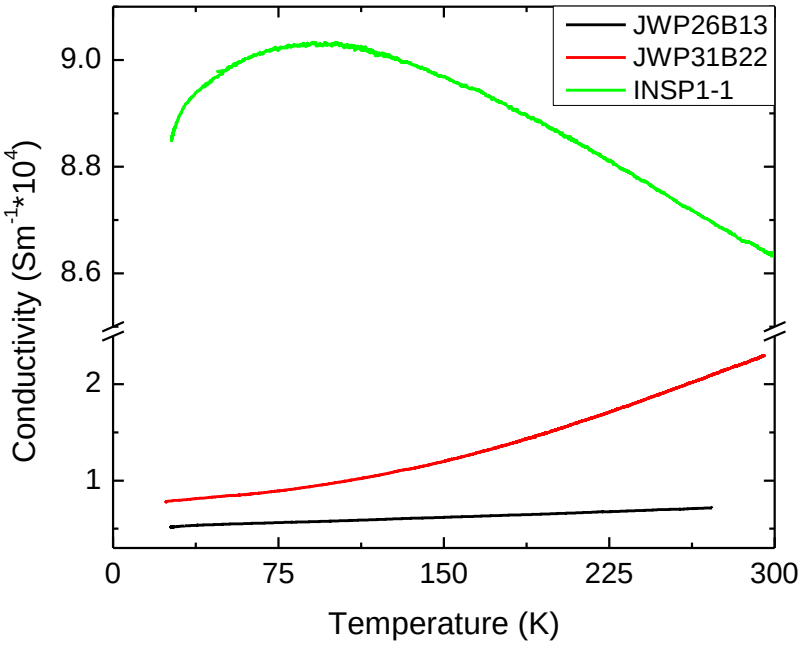

Fig. 21. Conductivity as a function of temperature of differently doped samples.

Spectrum photocurrent of InP nanowires with $5 \cdot 10^{18}\mathrm{cm}^{-3}$ doping was measured at room temperature and at 26K. Band gap of a semiconductor increases with decreasing temperature, due to the reduced vibrations of lattice atoms. This effect was observed in our measurement data (Fig. 22).

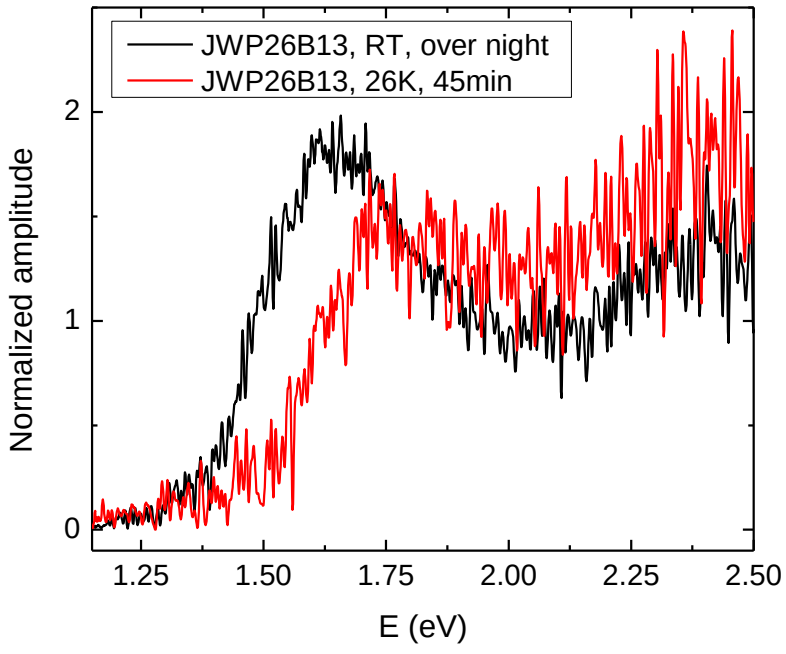

Fig. 22. JWP26B13 spectral photoconductivity at different temperatures.

With putting more dopant atoms to semiconductor, more states in conduction band are filled with electrons and Fermi level moves more deeply into the band. This phenomenon is known as state filling effect. Blue shift of photoluminescence (PL) peak due to the state filling, known as Burstein-Moss shift (see chapter 3.2), was observed in similar InP nanowires. Investigation of differently doped nanowires was performed by J. Wallentin, et al. [13]. However, their results do not fit with our measurement data where no blue-shift was observed (Fig. 23). On the other hand, the shift which was shown in the picture above is too big to be explained only with the band gap difference between 26K and room temperature, meaning that other phenomenon is doing influence to the spectrum, which cannot be seen at room temperature.

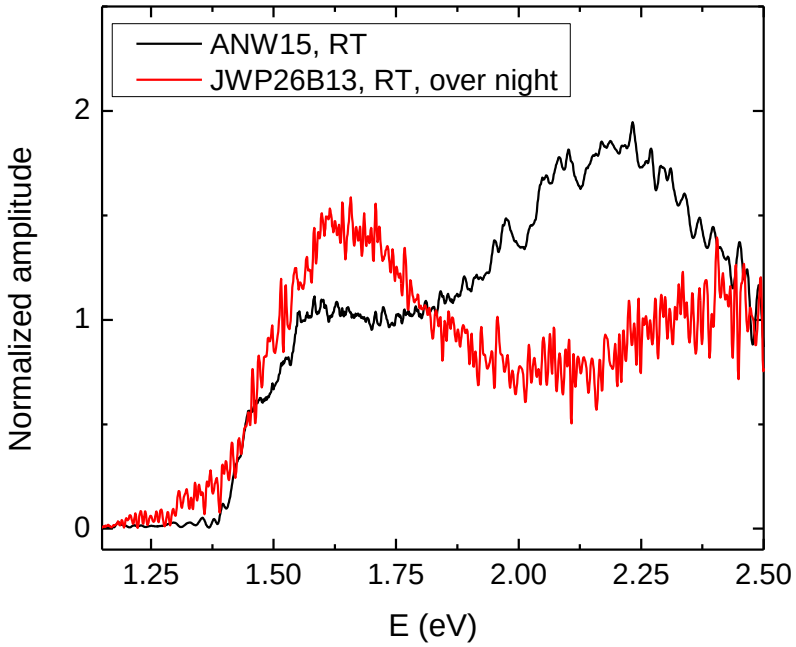

Fig. 23. Comparison of ANW15 and JWP2613 at room temperature.

One possible explanation of our results can be attributed to the electric field. In order to separate electron-hole pair bias was applied in spectral photoconductivity measurements. Then electrons in a conduction band are rearranged like it is shown in Fig. 24. In this case, lower energy photon is needed to excite electron to conduction band. Furthermore, interaction with phonon should have influence as well. On the other hand, different

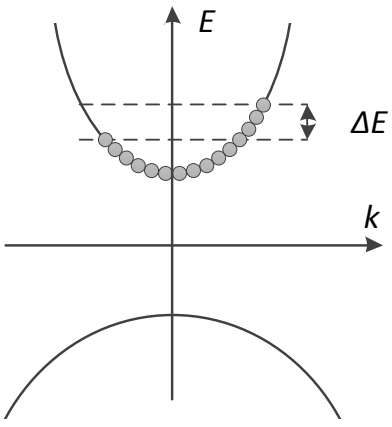

Fig. 24. Band structure of biased semiconductor.

drain source voltage should be applied at differently doped samples to avoid unfavorable effects related to high current. All things considered, experiments at low temperature and other measurements should be carried out to understand this phenomenon.

5.2. GaSb/InAsSb/InAs nanowire based IR photodetectors

As it was mentioned before InAsSb has the smallest band gap (~0.1eV at room temperature [15]) of all III-V semiconductors. Experiments with several different samples of GaSb/InAsSb/AsSb nanowire heterostructure were performed. The main aim of our studies was to measure spectral photocurrent of this structure and to investigate a band structure of these devices.

We have started with the single nanowire (see Fig. 13) measurements. Nanowires that showed the best diode IV characteristic had the biggest interest of ours. Diode rectification comes from GaSb and InAsSb junction. A plan was to use FTS and globar light source for low energies photocurrent measurements. IV characteristics in dark, with quartz and globar light sources gave promising results even in room temperature (current was higher when sample was illuminated). However, we could not get the spectral PC with globar. Several possible explanations can be proposed. One of them – a signal from single nanowire was not strong enough to measure due to too weak light source.

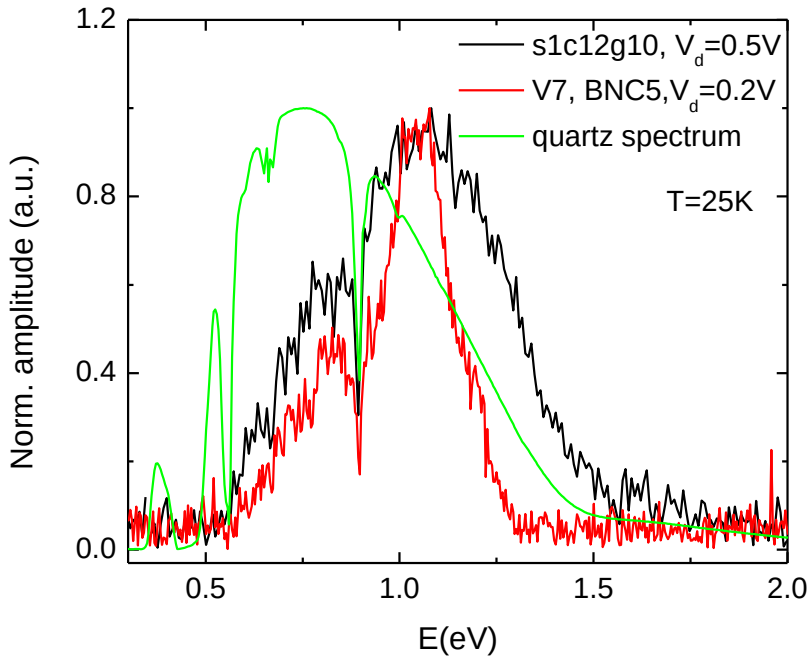

Fig. 25. Photocurrent as a function of energy of single (1c12g10) and multiple (V7) nanowire samples.

Spectral PC measured with quartz is shown in Fig. 25 (black curve). As it can be seen from the picture, PC was observed below GaSb band gap (0.81 eV at 25K). This means that other material (InAsSb or InAs) was absorbing light as well and it is very promising result. A drop of PC at higher energies can be explained comparing it with quartz spectrum, where incident light intensity decreases. According to SEM image (Fig. 13) this nanowire has no top GaSb segment. This means that photocurrent is generated in 5 nm thickness GaSb shell.

In order to have higher signal at lower energies, new samples of multiple nanowires were fabricated (Fig. 14). Wrong diode rectification was observed from IV measurements for most of the multiple nanowire samples. The origin of this unexpected result is still not explained**.** One of the reasons for this effect could be a direct contact to InAsSb instead of GaSb. Then junction between InAs and InAsSb becomes important even if it is a very similar material. Several wrong connected nanowires might be enough to see difference in I-V characteristic. Then difference in length of nanowires is a crucial aspect for correct sample fabrication. The solution for that might be longer GaSb segment.

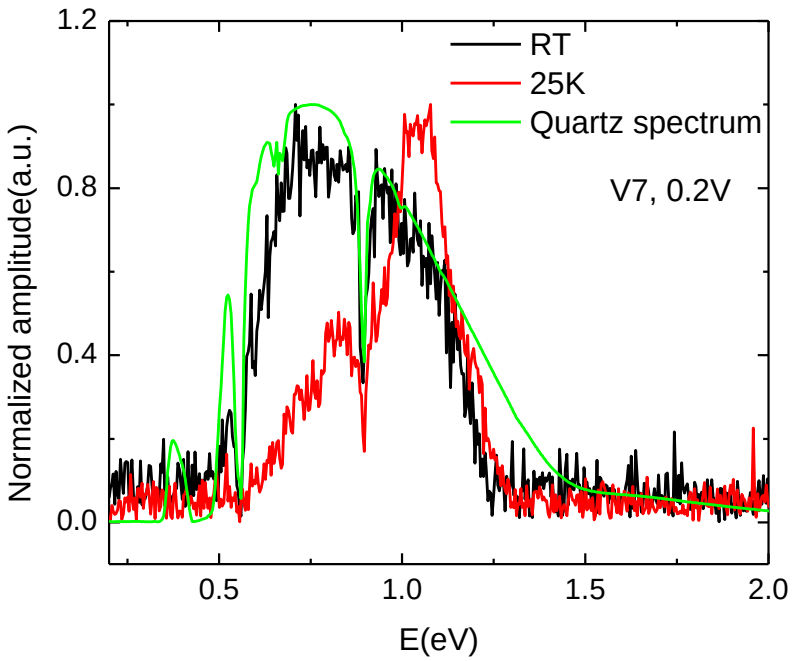

Fig. 26. Spectral PC of V7 using quartz light source at room temperature (black curve) and at 25K (red curve).

Spectral PC of multiple nanowire sample (V7) using quartz light source is shown in a Fig. 25 (red curve). It looks very similar to the single nanowire spectrum. Sharp cut-off at higher energies corresponds to the silicon band gap at 25K (silicon was used as a substrate for nanowires growth

(see Fig. 14)). Slightly lower signal of V7 at lower energies might be due to resist vertical wires were covered with.

Spectral PC of V7 using quartz light source at RT and 25K is shown in a picture below (Fig. 26). Spectrum measured at RT follows quartz spectrum quite well, except at higher energies, where Si starts to absorb light. Peak PC shift from 0.72eV (RT) to 0.81eV (25K) corresponds to the band gap of GaSb at these temperatures. Also, sharp slope is blue-shifted by approximately 0.05eV due to the change of silicon band gap. Furthermore, PC is not equal to zero at the energies smaller than GaSb bang gap. That indicates that carriers are generated in lower band gap semiconductor material.

Absorption in a sample with multiple vertical nanowires (V4) was measured. As it was mentioned before, the sample was placed on a ceramic sample holder with 2mm diameter hole in the middle for illumination from the back. Spectra were measured with DTGS detector. First of all, the sample holder without hole was placed in the path of the light to be sure that no light is coming around it. Then it was replaced with the sample holder with the hole to have a reference spectrum to compare it with identical sample holder with the sample on top of the hole. The results of all three measurements are shown in Fig. 27.

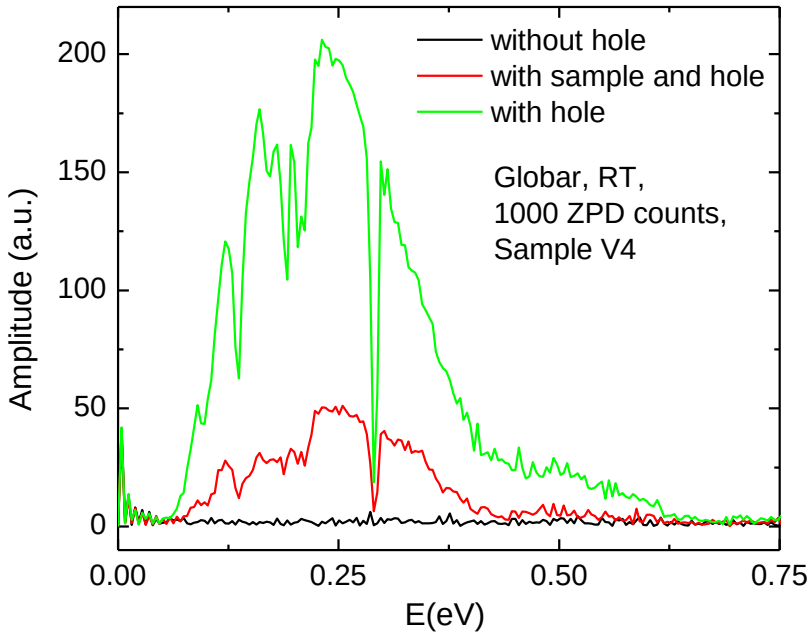

Fig. 27. Absorbtion measurements of sample hoder without hole (black curve), sample hoder with hole (green curve) and sample holder with hole and with sample (V4) on top (red curve).

Before analyzing results, the structure of the sample must be remembered. The top of the sample is covered with gold contacts (540 nm thickness) that are not transparent. Another factor that can make influence to the light is light scattering in resist or between interfaces of the surfaces

of different materials. Light with different wavelengths might be scattered differently and that could cause some uncertainties in measured spectrum. Due to these facts and absorption in the sample (probably too weak to see it), the spectrum measured with DGTS detector is much less intense.

Using globar light source spectral PC was observed (Fig. 28). Due to a very weak signal measurement time was increased drastically. At RT band gap of InAs and InAsSb with 10% of Sb is 0.35 eV and 0.29 eV, respectively. Because of bad signal-to-noise ratio it is hard to estimate correctly where the peak starts to grow, but most probably it corresponds to carrier excitation over InAs band gap and InAsSb photocurrent input to spectrum is minor. Smaller peak at higher energies can be attributed to silicon substrate. Here carriers generated in silicon diffused to *n*-doped InAs layer. Even if light intensity of globar at that energy is very low, silicon substrate is quite thick and due to long measurement arise of this peak might be determined.

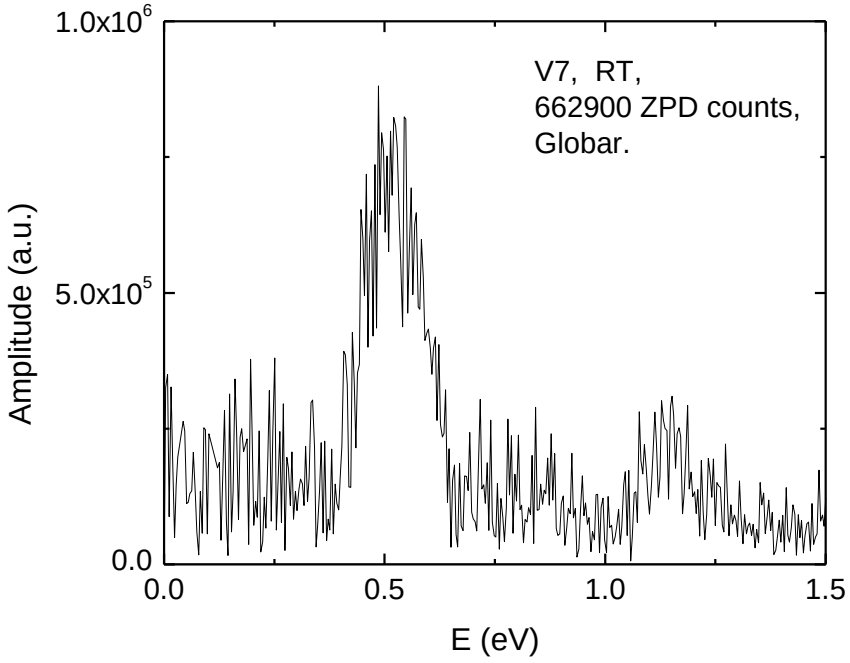

Fig. 28. Spectral PC of V7 sample using globar light source.

In order to see if thin InAs layer (5 nm) used as a back contact absorb light, spectral PC was measured. In this case, two contacts on InAs were biased while illuminated with modulated light (FTIR). Experimental results are shown in a picture below (Fig. 29). No broad spectrum starting at higher energies than InAs band gap was observed. This indicates that the InAs layer is too thin to make visible influence on incident light. However, sharp and strong peak can be seen in higher energies. This is due to the silicon substrate. It has high resistivity, so no insulating layer between silicon and InAs is needed.

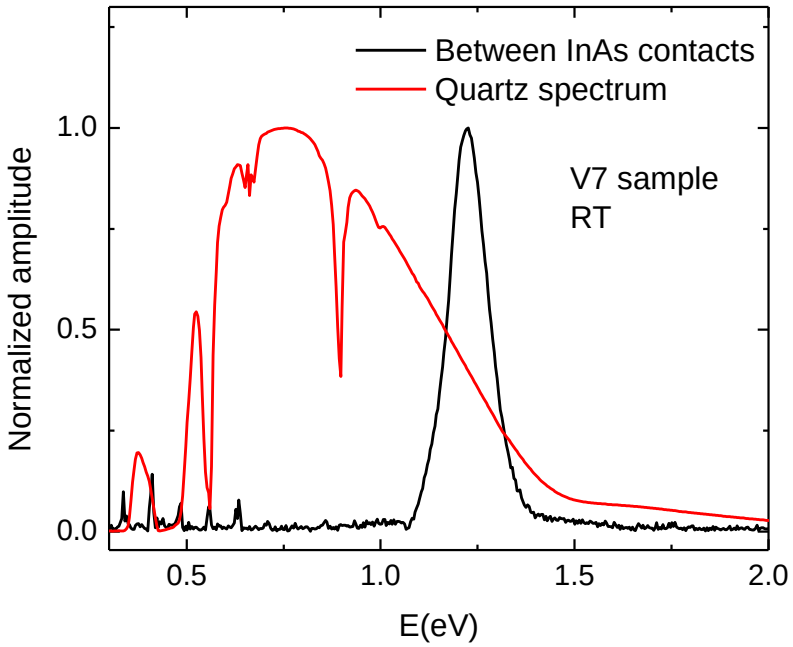

Fig. 29. Spectral photocurrent when two contacts on top of InAs is biased.

An interesting result was observing this sharp peak even when the sample was unbiased. This indicates another carrier transport mechanism - diffusion. Carriers generated with light due to the high concentration diffuse out of illumination spot. If only one contact was illuminated, then in there we have more carriers than in other and that may give us spectrum at zero bias.

5.3. InP LED results

Optical properties of indium phosphide nanowire based light emitting diodes were investigated. Unfortunately, these devices did not show good diode behavior (Fig. 30). This might be due to the leakage through SiO_2. Despite of this fact, electroluminescence experiments were performed.

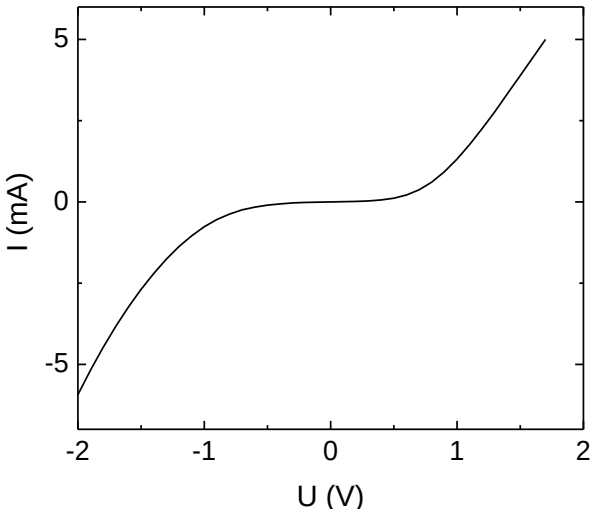

Fig. 30. IV characteristic of D6 device.

Using microscope (with 100x magnification objective lens) and CCD camera some images showing emission of light were taken (Fig. 31 and Fig. 32). An important fact is

CCD sensitivity for infrared light. At the region of interest it has approximately 7% quantum efficiency. Due to this issue exposure time was increased to 60 seconds.

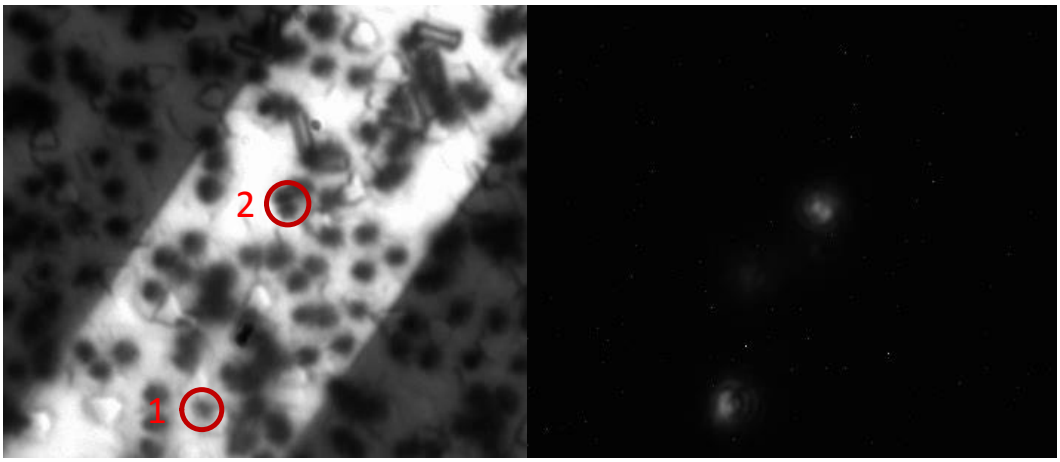

Fig. 31. Image of sample D6 and electroluminescence when 2.5V bias applied.

Some of the devices did not show electroluminescence on repeated experiment measurement (Fig. 32), meaning that these devices are not stable. This could be caused by insulator (SiO_2) electrical break due to the non-uniform thickness.

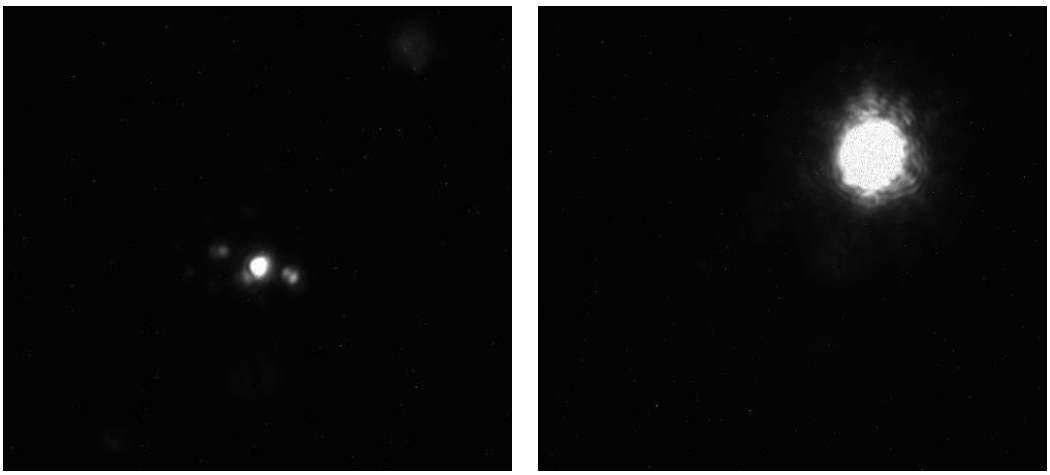

a b

Fig. 32. Electroluminescence of D39 (a) and D18 (b).

Spectral measurements were performed at room temperature using grating spectrometer. Two spectra of marked nanowires (see Fig. 31) are shown in a picture below (Fig. 33). Two peaks at 1.46 eV and 1.57 eV are visible as well as very broad electroluminescence spectrum.

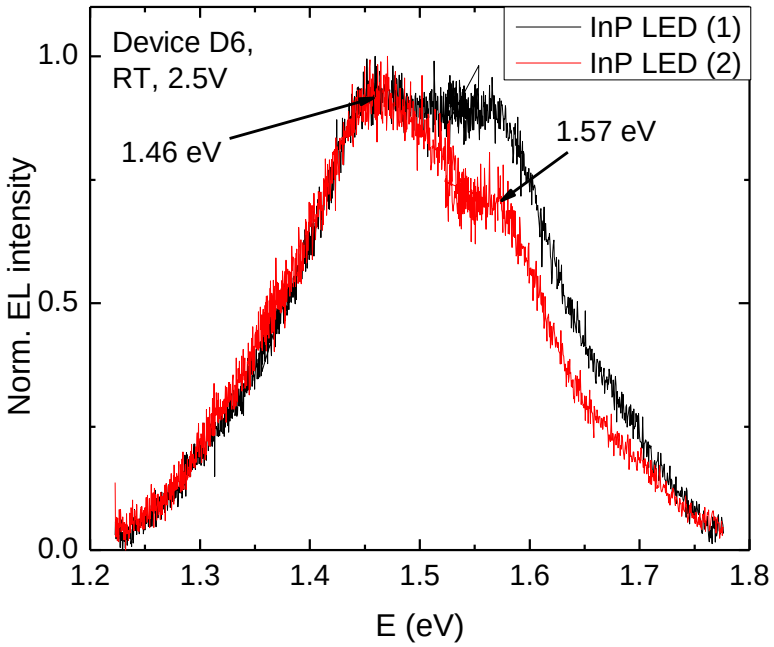

Fig. 33. Electroluminescence spectrum of D6 device.

The photoluminescence peak of InP/InAsP/InP quantum well shifts towards higher energies when thickness of the quantum well decreases [18]. According to the structure of the device, the peak of 2 nm quantum well should appear at 1.45eV at low temperatures. Our measurements were performed at room temperature. This means that peak must be shifted to lower energies roughly by 0.1 eV. However, no peak was observed there. Since this QW is so thin (2nm), a slight change in thickness may cause big change of energy of the subbands. And due to hexagonal shape of QW, in the corners it is thicker than in other parts. This corresponds to the lower energy of the subband. So, when carriers are injected to QW, first of all they occupy lowest energy states. This effect is visible in the measured spectrum as a long tail towards lower energies.

During experiment 2.5 V bias was applied and around 4 mA current was flowing through the device. Due to this big carrier injection to device state filling effect and Burstein-Moss shift might occur. This effect might be responsible for the second peak and tail to higher energies where two different parts in a slope can be seen. Influence to the spectrum at higher energies might be caused by carrier transitions from second conduction band, where states are filled due to high electrical carrier injection. In WZ InP the second conduction band is only 0.24eV higher than the first one.

6. Conclusions

1. No significant change in photoconductivity of InP nanowires was observed with changing temperature in both cases of high and low illumination power, meaning minor influence of phonon scattering to conductivity or misinterpreting results due to SC heating issue.

2. Conductivity dependence on temperature of differently doped InP nanowires has shown semiconductor behavior (conductivity increased with decreasing energy), except most heavily doped (inps1-1) sample where metallic (T>86K) and semiconductor (T<86K) dependences were observed.

3. No blue shift, corresponding to state filling, was observed with increasing doping of InP nanowires, which is still not well understood.

4. Weak photoresponce to far infrared light of GaSb/InAsSb/InAs photodetectors could be caused by few factors:

a) lack of active region material;

b) illumination from the back side of the sample might have some negative aspects, such as only radial area being in the way of light instead of whole length of nanowire, which would be in the case of side illumination.

5. Wrong rectification of GaSb/InAsSb/InAs could be caused by InAsSb/InAs junction because of contacting directly to the InAsSb. To avoid it, longer GaSb top segment should be grown.

6. Broad electroluminescence spectrum of investigated InP nanowire based LEDs with radial InP/InAsP/InP quantum well can be attributed to two basic phenomena: inhomogeneous thickness of quantum well gives tail to lower energies and strong state filling effect due to high electrical carrier injection to the active region.

7. Leakage and minority of working and light emitting nanowire LEDs indicates low reliability of these devices. More careful fabrication process and fabrication of ordered nanowire devices should be done.

All in all, it was shown that experimental methods we have used can be very useful for the semiconductor nanowires investigation. However, some interesting questions brought by our measurements should be answered in the future.

7. Acknowledgement

Special thanks for my supervisor Dan Hessman for interesting discussions and guidance through difficulties that occurred. Also, I want to thank Simon Zihlmann for his collaboration and good mood during this project. Big thanks for Johannes Svensson for nanowire growth, sample fabrication, SEM images and his optimism. I also appreciate advices and help from David Lindgren, Mats-Erik Pistol and other people in department.

8. References

1. Schubert E. F. (2003). Light-Emitting Diodes, Cambridge: Cambridge University Press.
2. Sze S. M., Kwok K. Ng. (2007). Physics of Semiconductor Devices. John Willey & Sons.
3. Grundmann M. (2010). The Physics of Semiconductors. Springer.
4. Streetman B. G., Banerjee S. K. (2009). Solid State Electronic Devices. Pearson Prentice Hall.
5. Davis S. P., Abrams M. C., Brault J. W. (2001). Fourier Transform Spectrometry. Academic Press, USA.
6. Griffiths P. R., de Haseth J. A. (2007). Fourier Transform Infrared Spectrometry. John Willey & Sons.
7. Wunch D. (2006). Measurements and Data Analysis from a Balloon-Borne Fourier Transform Spectrometer. University of Toronto (PhD thesis).
8. Forman M.L., Steel W.H., Vanasse G. A. (1966). Correction of Asymmetric Interferograms Obtained in Fourier Spectroscopy. *Journal of the Optical Society of America*, 56, 59-63.
9. Wunch D. (2006). University of Toronto's balloon-borne Gourier transform spectrometer. *Review of Scientific Instruments*, 77, 093104.
10. Jansson A. (2011). Photoconductivity in Single Nanowires (Master Thesis).
11. http://www.ioffe.ru/SVA/NSM/Semicond/InP/bandstr.html, 2011-12-20.
12. Jansu J.-M, et. Al.(2010). Type II Heterostructure Formed by Zinc-blende Inclusions in InP and GaAs Wurtzite Nanowires. *Applied Physics Letters*, 97, 041910.

13. Wallentin J., et al. (2011). Probing the Wurtzite Conduction Band Structure Using State Filing in Highly Doped InP Nanowires. *Nano Letters*, 11, 2286-2290.

14. Wallentin J., et al. (2011). Electron Trapping in InP Nanowire FETs with Stacking Faults. *Nano Letters*, Article ASAP.

15. Svensson J. (2011). Heterostructure nanowires for detection of infrared radiation (Research program).

16. Tuin G.L. (2010). Optical Characterization of Wurtzite Indium Phosphide (Master Thesis).

17. Vurgaftman I., Meyer J.R., Ram-Mohan L.R. (2001). Band Parameters for III-V compound semiconductors and their alloys. *J. of Appl. Phys*., 89, 5815-5675.

18. Kawaguchi K., Heurlin M., Lindgren D., Borgström M.T., Samuelson L. (2011). MOVPE Growth and Optical Properties of Wurtzite InP Nanowires with Radial InP/InAsP Quantum Wells, *23rd International Conference of Indium Phosphide and Related Materials*. Berlin, Germany.

19. Minot, E. D., et al. (2007). Single Quantum Dot Nanowire LEDs. *Nano letters*, 7 (2), 367-371.